Journal of Achievements in Materials and Manufacturing Engineering
VOLUME 24
ISSUE 1
September
2007

Damage mechanisms of Ti-Al intermetallics in three point ultrasonic bending fatigue

E. Bayraktar [a,*]
co-operating with
H. Xue [b], C. Bathias [c]
[a] Supmeca/LISMMA -Paris, School of Mechanical & Manufacturing Engineering, France
[b] Northwestern Polytechnical University,
School of Aircraft Design Engineering, Xi'an, China
[c] ITMA- CNAM, School of Mechanical Engineering, Paris, France
* Corresponding author: E-mail address: bayraktar@supmeca.fr

Received 20.03.2007; published in revised form 01.09.2007

Properties

ABSTRACT

Purpose: Damage mechanisms of two phases (α_2-Ti_3Al and γ−Ti-Al) intermetallics alloy are investigated at room temperature in a new developed resonance type 3- point (3P) fatigue bending test device at a frequency of 20 kHz.
Design/methodology/approach: Manufacturing and analysis of composition of this alloy were carried out in advanced materials laboratory by collaborating with aircraft design engineering department for non-ferrous metal research centre in China. All of the 3P- fatigue bending were carried out at the stress ratios of R=0.1, R=0.5, R=0.7 mainly in gigacycle regime.
Findings: Damage mechanisms were compared in static and dynamic test conditions. The geometries of static tensile test and ultrasonic fatigue test specimens have been calculated by analytical or numerical method as discussed in detail formerly. This paper gives further results and more complicate discussion on this study particularly on the crack formation and the role of the different parameters on the damage mechanisms of this alloy. Damage analysis was made by means of optical (OM) and Scanning Electron Microscopies (SEM).
Research limitations/implications: Paper gives results and more complicate discussion on the crack formation and the role of the different parameters on the damage mechanisms of this alloy.
Originality/value: This study proposes a new methodology for fatigue design and a new idea on the criterion for the damage under very high cycle fatigue regime. The results are well comparables for the specimens under real service conditions. This type of study gives many facilities for the sake of simplicity in industrial application.
Keywords: Gigacycle fatigue; binary phase Ti-Al (α2+ γ) alloy; Damage mechanism; Ultrasonic fatigue bending test

1. Introduction

Light alloys based on γ + α_2 phases are considered as very potential materials for lightweight high-temperature structural applications essentially in aerospace such as gas turbine and in thermal protection systems because of their low density, high temperature strength, oxidation resistance and low thermal conductivity [1-5, 7-16]. They are very performance materials at high operating temperature up to ~750°C such as some of the components of aircraft turbine, which crack around 10^{10} cycles. Application of these materials is limited, however, by low temperature ductility and questionable fatigue crack growth resistance.

As an promising structural material, α_2 phase in binary phase Ti-Al (α_2 + γ) is distributed in γ phase, it has ordered $D0_{19}$ structure, it is a brittle phase, cleavage rupture occurs in α_2 phase. Besides, the ductility of the Ti-Al-based alloy is relevant to the composition of oxygen, α_2 phase can solute much more oxygen than γ phase, and the deformation of the alloy is depended on the γ phase, the reduce of oxygen in the γ phase is useful to improve the ductility [1, 3-9, 15-19].

Mechanical performance of this alloy is depended on their microstructure. Usually, Ti-Al alloy is divided into four typical microstructures; equiaxed γ-grains, Duplex microstructure (DP), nearly lamellar microstructure (NFL) and fully lamellar microstructure (FL). Equiaxed γ-grains is composed of great deal of large γ-grains and a little α_2 grains, DP microstructure is composed of the same fraction small γ-grains and γ/α_2 lamellar colonies (40-100μm), the grains of DP microstructure are smaller. A great deal of γ/α_2 lamellar colonies and small part of equiaxed γ grains composed NFL microstructure; for the FL microstructure, it only has big γ/α_2 lamellar colonies. The typical microstructure of binary phase Ti-Al based alloys are DP and FL microstructure. The mechanical performance of the Ti-Al-based alloy is mainly governed by their microstructure factors, specifically, colony size, lamellar spacing, colony boundary characteristics, and fraction of γ/α_2 lamellar colonies [20-23].

Previous investigations have revealed that the measured fracture and fatigue properties of lamellar microstructures are functions of the geometry and the size of the specimen [1-14]. It is known that addition of the Nb at the level of 5-10 at. % to this material may improve the strength of Ti-Al base alloys by refining of the microstructure [4, 5, 8]. Recently, A detail study on the gigacycle 3P - bending - fatigue failure behaviour of two phases ($\gamma+\alpha_2$) Ti-Al alloy were published [9]. However, this paper gives further results and more complicate discussion on this study particularly on the crack formation and the role of the different parameters on the damage mechanisms of this alloy.

2. Manufacturing of Ti-Al alloy in advanced materials laboratory

The chemical composition of the alloy is given as (at %) Ti-45Al-8.5Nb-0.2W-0.2Mo-0.3B. Firstly, this alloy was produced by vacuum electric arc melting, after twice melting and then it was shaped. All of the manufacturing stages were carried out in advanced materials laboratory by collaborating with aircraft design engineering department for non-ferrous metal research section in China. The original material included 0# sponge titanium, very high pure aluminum bar, “Al-74.5Nb alloy”, “W” powder and so on. Melting has been carried out from 5kg original material according to the composition to obtain ∅ 90mm cast ingot. Cast ingot was then re-melted two times so as to get the well-balanced cast bar. In order to remove the shrinkage porosity in cast material and also to obtain the uniformity compact structure, the cast ingot had been processed by hot isostatic pressing (HIP) at a pressure of 175MPa and a temperature of 1200˚C for 12h, then after, was cooled with the electric furnace. This stage was important in manufacturing process [19].

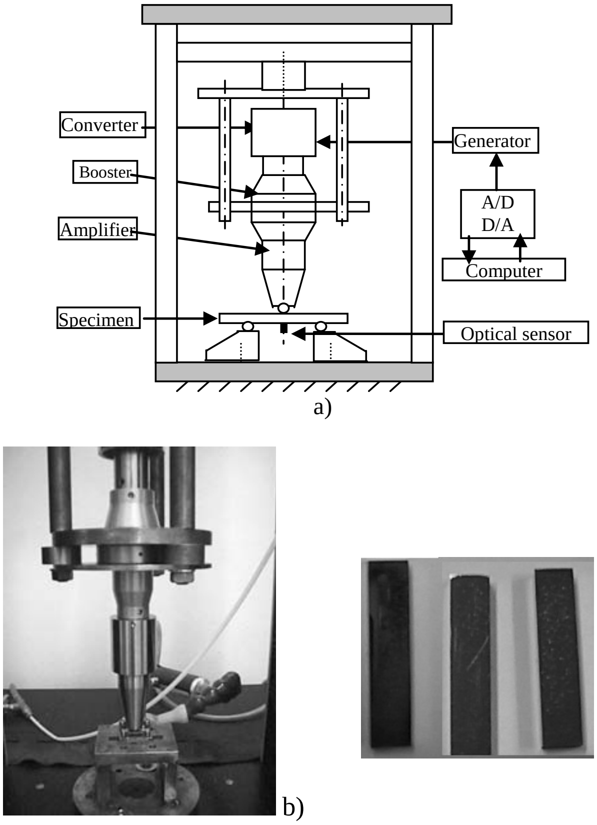

Fig. 1. Schematic description a) of three-point bending fatigue test device and manufactured test samples, b)

In order to verify the homogeneous degree of the cast ingot composition, the chemical composition and phases were analyzed. Table 1 shows these results. It revels that the composition of the cast ingot is uniformity. Figure 1a and b shows the description of three-point bending fatigue test device (A resonance type) and manufactured test samples. Metallographic samples were then taken from the cast bar of the Ti-Al based alloy specimens by means of EDM cutting in longitudinal and vertical direction with respect to the main centre line of the bar. Optical micrographs of the Ti-Al alloy longitudinal section of the test specimen and chemical (EDS) analyzing of phases taken by means of the optical microscope (OM) was given in Figure 2.

As will be seen in the next section in detail, the microstructure of the alloy is composed of the colonies of the full lamellar microstructure. For this structural analysis, specimens were cut from the gage sections out of the fatigue fractured specimens that they were taken very close to the fracture surface. The results have confirmed that fully lamellar structure is composed of $D0_{19}$ structure α_2 phase and $L1_0$ structure γ phase.

Table 1.
Compostion of the specimens desined for the test

Composition	Ti	Al	Nb	Mo	W	B
Design-average	52.5	27.62	19.87	0.22	0.22	0.1

The size of the colony is 80-200μm, the lamellar spacing is 2-4μm, and some γ grains exist in the boundary of the colonies. The interdendritic regions rich in Al after casting are leading to a small volume fraction of single phase γ.
Some of this interdendritic γ-phase is retained after HIP followed by heat treatment. Both of them are situated between and/or within the large lamellar colonies. Most of the specimen showed that, γ-phase was situated in the colony boundaries. However, small γ-regions without any distinguished grain boundaries can be seen in the interior of some lamellar colonies.

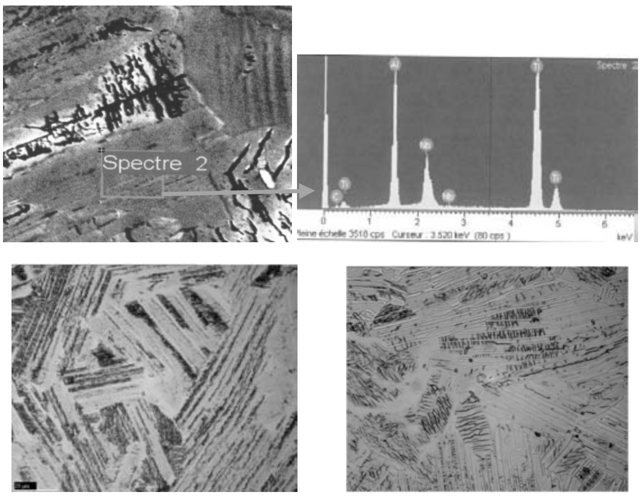

Fig. 2. Optical micrographs of of the Ti-Al alloy longitudinal section of the test specimen and chemical analyzing of phases

3. Design of the specimens

The specimens used for static three point (3P) bending and ultrasonic bending fatigue tests are shown in Figure 3a and b. According to the research objective in this study, two groups of specimens with different geometry were designed:
I- The geometry of ultrasonic fatigue specimen has been calculated by analytical or numerical method (ANSYS-VI) as discussed in detail in the former papers [9, 10].
II- The geometry of the Ti-Al based alloy specimen for static tensile test was displayed in Figure 3c [10].
Rectangular specimens were cut from the rod with a diameter of 90mm using electro discharge machining (EDM) according the design results. Each specimen was then mechanically polished to improve surface quality before testing. So, initial surface roughness was measured below the value of 3μm. In order to observe the crack evolution very clearly, some specimens were polished using SiC paper plus diamond powder and then etched the surface of the specimens.

4. Testing and calibration procedures

Static tensile and bending tests have been carried out for determining mechanical properties of the Ti-Al intermetallics alloy; three-point bending ultrasonic fatigue test has been conducted for determining high cycle fatigue properties. All of these tests aimed to explain the damage mechanism of this alloy.
I. Tensile test: The polished static tensile samples were tested at the loading rate is 0.2mm/min.
II. Static bending test: Static bending specimens were used to measure the bending strength with smooth specimens and some of them were notched to observe the crack evolution.
III. Ultrasonic fatigue test: Three-point bending fatigue test was conducted in a specially developed ultrasonic fatigue test device controlled by the maximum vibration displacement at the centre of the specimen.

All of the tests were performed at ambient temperature with a frequency of 20 kHz. Static stress was loaded by INSTRON 1122 fatigue machine. The fatigue tests with the stress ratios of R=0.1, R=0.5 and R=0.7 in the range of 10^5-10^{10} cycles were carried out. Compressed air was used in the ultrasonic fatigue test, so as to avoid the influence of the temperature on the fatigue properties (Figure 1). A resonance type fatigue-testing device was given in. SEM, JOEL-Cambridge 20kV was used to study fractography and damage mechanism in 3P-bending fatigue failure.

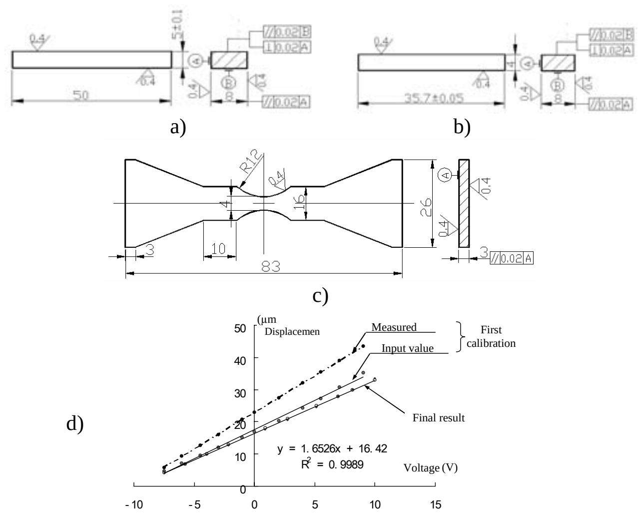

Fig. 3. Geometries of the specimens in bending a), fatigue b), tension c) and the calibration of the system before fatigue test d)

The SINAPTEC optical sensor was used in calibrating the fatigue vibration system; precision of the measurement is 0.1μm, the measure range is a range of 1-199.9µm and the frequency is a range of 3Hz-70 kHz Figure 3d.. The calibration process of the system should be checked every time to control the parameter by comparing the results obtained from optical sensor with the one input by means of the computer (less than 1%). Calibration process should be repeated to obtain the reasonable parameter.

5. Results and discussion

5.1. Microstructure

The microstructure is nearly lamellar structure with a grain size of 100µm and a lamellar spacing of 2-4µm. Lamellar colony contains γ-ordered fcc (111) based tetragonal and very fine α_2 - Ti_3Al (0001) ordered hcp platelets and a few small grains of γ Ti-Al structure (~ 4-10µm) respectively (Figure 4a and b). Neither pore nor grain boundary precipitation were observed in the specimens studied. They illustrate an intensive twin formation in the microstructure (in γ grains as well as in lamellar grains) of the specimens tested at different conditions (static bending and ultrasonic fatigue tests). In fact, twin density is higher in static bending specimens than that of the 3P- bending fatigue. It should be however noted that the static bending test and 3P-bending fatigue test can not be compared directly because of the difference of the modes. But, these results should be accepted as indicative for understanding the mechanical twin formation in this alloy. Early studies showed that twins influence strongly the damage mechanism of this intermetallics alloy at ambient and high temperature [10-14]. They demonstrated that twinning mechanism can easily occurred at lower stress levels well under the elastic limit. They found that the critical resolved shear stress (described by Schmidt’s law) is larger than that of simple dislocation glide and a little lower than that of super dislocation glide. They showed also that twins nucleate mainly within the grain by a pole mechanism due to a partial dislocation turning around a perfect dislocation.

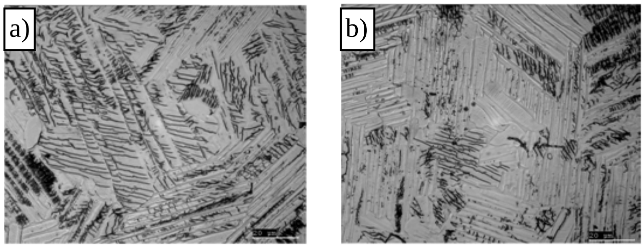

Fig. 4. Formation of intensive twins after the static bending test a) and after the fatigue test at the stress ratio of R = 0.5 b)

5.2. Tensile and bending tests

Table 2 indicates tensile properties of the specimens. During the test, any yield step is observed in the stress-strain curve with an elongation ratio of 0.53% for the Ti-Al based alloy that shows a typical brittle fracture characteristic. Although the ultimate tensile strength (UTS) is only 500MPa, elastic modulus (E) is 161GPa, the ratio (the performance indices, I_p,) of strength and elastic modulus to the mass are higher than structural steel.

As explained in the former section, the bending specimens were also processed from the cast ingot by hot isostatic pressing (HIP). The bending test results are also given in Table 2. It shows that the flexural strength is 850MPa. This value is higher than with respect to the conventional process that does not contain a HIP stage.

Table 2.
Tensile and Bending test results

Mean values	Applied load (kN)	UTS (MPa)	Elastic Modulus E (GPa)	δ%
Tensile test	5.835	500	161	0.53
Bending test	3.702	850		

The static bending fracture surfaces given in Figure 5a and b shows mixed of intergranular and transgranular fracture (a) and typical transgranular cleavage (b). The uniform lamellar orientation existing in a single lamellae colony encourages crystallographic crack propagation by taking the same direction in one colony. In this case, the crack tends to propagate with a quite low angle of crack plane to the lamellar laths and a resulting transgranular fracture. Additionally, when the crack tip come across the colony boundaries, the cracks did not propagate along a single lamellar lath interfaces but the crack propagates along the colony boundaries, thus it causes the intergranular fracture in some cases. For the Ti-Al intermetallics, due to the high strength of the α_2 lath and narrow lamellar lath spacing, crack can occur occasionally rather than constantly. As a result, the crack does not propagate at all along a single lamellar lath interface. They frequently had a tendency to jump to adjacent or in another lamellar lath interfaces by branching. The path of crack propagation is a bending type. Ti-Al intermetallics having a lamellar structure have higher bending strength.

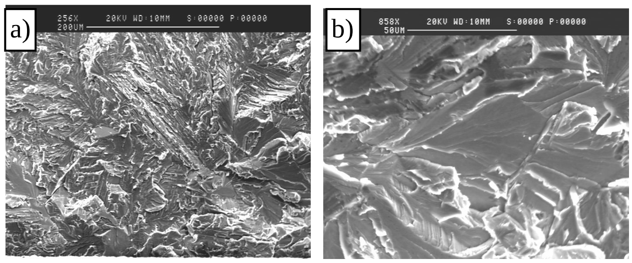

Fig. 5. Static 3P bending fracture surfaces, (a) mixed of intergranular and transgranular fracture (b) transgranular cleavage

5.3. Fatigue properties

Ultrasonic fatigue bending properties explained by S-N curves were evaluated for three different stress ratios of 0.1, 0.5 and 0.7 respectively. They show the elastic nominal peak stress at the outer of the beam versus the number of cycles to failure. Specimens, which did not fail, are marked with arrowhead.

In order to understand the influence of surface roughness on the fatigue properties, the fatigue specimens have been prepared in different surface roughness conditions. According to the surface roughness values, they were classified into three groups as follows: surface roughness is (1) less 0.5µm called fine; (2) 0.5-

1.5µm called medium and (3) 1.5-3µm called coarse. This type of evaluation has been carried out only for a stress ratio of R= 0.7.

These experimental results are given in Figure 6 show that the fracture of the most of the specimens occurred between 10^6-10^9 cycles. Fatigue life beyond 10^7 cycles gave a weak slope with a fatigue value at the level of 670MPa.

To evaluate the effect of stress ratio on the fatigue behaviour of this alloy, S-N curves have been presented at three different stress ratios together in Figure 7.

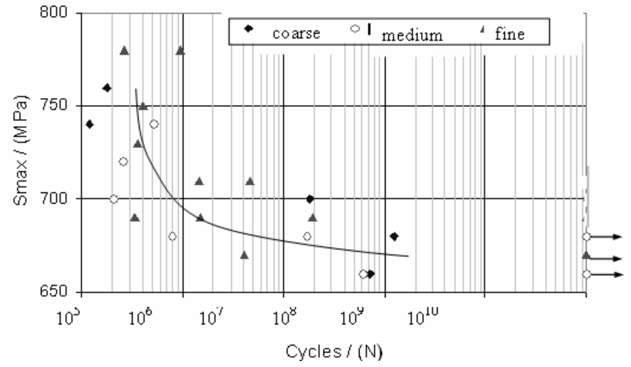

Fig. 6. Surface roughness effect on the S-N curve of Ti-Al intermetallics (R=0.7)

As observed from the Figure 6, these experimental results obtained with the specimens having different surface roughness indicate that there is no noticeable effect of surface roughness of the specimen on the fatigue life in our experimental conditions. Surface roughness conditions do not play an efficient role on the fatigue life particularly in the high cycle regime.

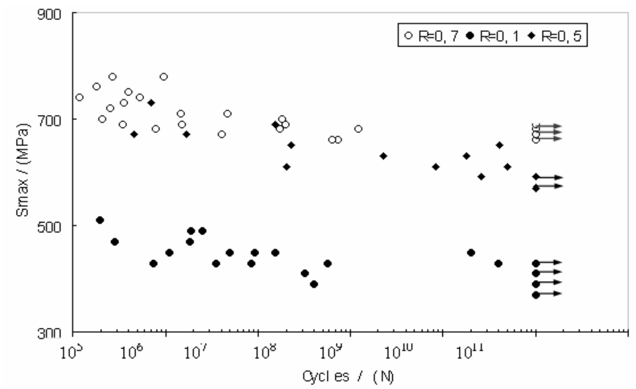

Fig. 7. Comparison of fatigue bending test results with the stress ratios of R=0.1, R=0.5 and R=0.7 respectively

It is seen that the dispersion in values obtained is considerable for three different stress ratio under the same nominal peak stress and these results are typical for showing the fatigue behaviour of this alloy with full lamellar structure in very high cycle regime. In the case of R= 0.1, many of fracture occurred between 10^7- $5x10^8$ cycles and S-N curve indicates a very slender slope. Fatigue strength beyond 10^9 cycles is 395 MPa. But, in the case of R=0.5, many specimens were failed over 10^7 cycles and also some of the specimens failed over 10^9 cycles. High stress ratio (R=0.5) can encourage fatigue fracture of specimens in the very high cycles regime. However, when the nominal peak stress is close to the static bending stress (in the case of R=0.7), many of the fatigue specimens failed in very low cycles regime while, the fatigue test data obtained with stress ratios of R= 0.1 and R= 0.5 have distributed in a wide cycle ranges.

5.4. Damage mechanism under static three point bending test

Fractography analysis has been carried out on the smooth and notched static 3P bend test for specimens. The initiation of the surface crack profiles and fracture surface of the specimens tested at room temperature were evaluated. Fracture surfaces of these specimens (SEM) are indicated in Figure 8. Essentially, transgranular and translamellar fracture surfaces are observed.

Moreover, this type of fracture surfaces requires evaluating the crack nucleation and growth, each side of the specimens by SEM. Figure 9 shows how most of the cracks initiated and followed labyrinthine crack paths in the notch specimen. Crack growth is occurred irregularly and crack initiation takes place parallel to the lamellar interfaces. Meanwhile, many new small cracks resulted in the crack deflection and/or crack deviation through an adjacent lamellar colony (i.e. cracks-branching). There is no considerable difference in the fracture behaviour between smooth and notched specimens.

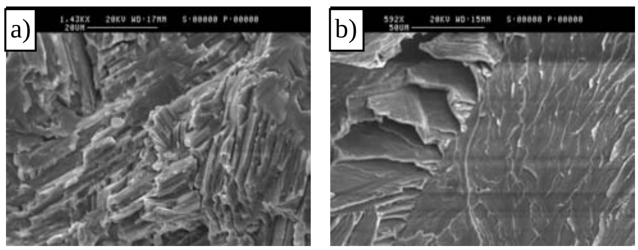

Fig. 8. SEM micrographs; static 3P bending fracture surfaces transgranular fracture a) and translamellar fracture surface b)

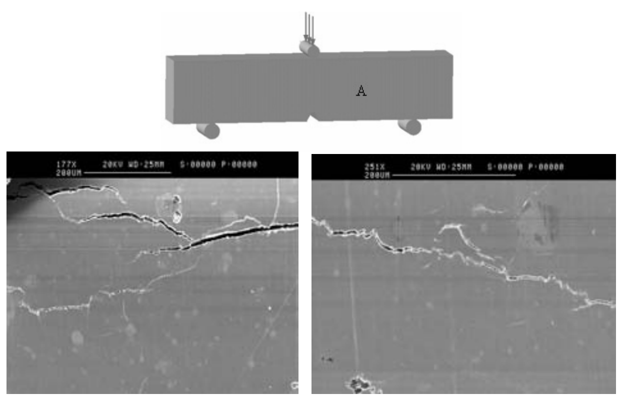

Fig. 9. SEM micrographs showing crack evolution with different lamellar orientation

5.5. Damage mechanism under three point ultrasonic fatigue bending test

Damage mechanism from fractography carried out on the fatigue test (smooth) specimens at three different stress ratios was also evaluated. Generally, fracture initiation were observed at the surface or subsurface of the specimen where the stress were highest, and it indicates that translamellar fracture start at weak interfaces by de-cohesion of lamellae parallel to the fracture surface and then propagates very rapid with small subcracks. Many secondary cracks sustained perpendicularly from fracture surfaces and were arrested during their evolution by the adverse lamellae orientations. Many fracture surfaces of these specimens failed in high cycle ranges that they have displayed by very small local micro plastic deformation zones. Our observations in this study are agreed with former results [4, 7, 9, 20].

Fatigue crack evolution and fracture surfaces of specimens tested at R= 0.1, 0.5 and 0.7 were presented in Figures 10 to 16. For the fatigue specimen in very high cycle regime (>10^7 cycles), fatigue crack pattern is generally translamellar and irregularly interlamellar sometimes with a large facets in the fatigue initiation. Subsurface fatigue initiation side started from the second phase or from a micro void was also determined in some of the specimens failed beyond 10^7 cycles. First of all, fatigue damage mechanism is an initiation type for the smooth and notched specimens.

More addition, detail information and the position of the slip bands in basal plane with secondary short cracks with large facets have been illustrated in Figure 10. It can be supposed that these should result in considerable local stress mismatching which lead to the final fracture of the material. Crack initiation and evolution takes place essentially by slip plane cracking (Figure 10d) which displays a typical step wise slip plane. This type of stair step fracture continued as a main crack growth pattern as explained in the former sections.

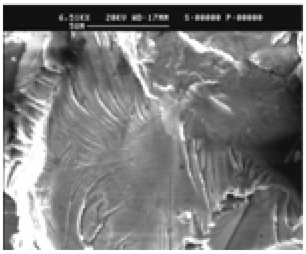
a) R = 0.1, N_f =1.5* 10^8


b) R = 0.1, N_f = 1.82*10^8


c) R = 0.5, N_f = 8.33*10^8


d) R=0.1, N_f= 1x10^7

Fig. 10. SEM micrographs, formation of slip bands in basal plane with secondary short cracks in large facets

In fact, observations of mechanical twins can be easily carried out by SEM. However, more detail TEM investigations (quantitative analysis of twins, etc...) are necessary to study this phenomenon.

At the first estimation, Mechanical twins form very early at the surface of the specimens essentially on the compression side. Mechanical twinning becomes a preferable mode of deformation because of the low stacking fault energy in this alloy. Therefore, it appears at the early beginning of the test by providing an additional deformation mechanism in gigacycle fatigue range and becomes favourable mechanism for increasing the fatigue life (toughening effect).

After that, many small cracks are produced but only a few of them may develop up to the final fracture. In other words, twinning contributes to deformation by crystallographic glide and by emitting ordinary dislocations, which may contribute to further deformation by increasing the lifetime.

Finally, real crack formations, which govern the fatigue damage, are seen on the outside of the specimens due to the tensile forces in this side. Thus, the crack formation process of the failed fatigue specimens using SEM was illustrated in Figure 11 for both of two stress ratios of R = 0.1 and 0.5 respectively. These observations by SEM indicate evidently crack branching with many micro cracks and crack deflection in this alloys.

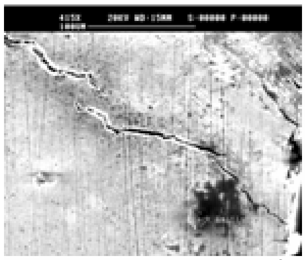
a) R = 0.5, N_f = 8.33*10^8


b) R = 0.1, N_f = 8.33*10^8

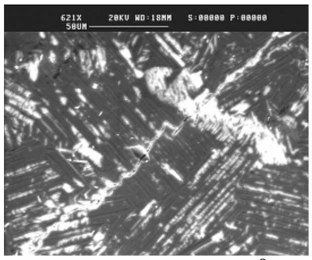
c) R = 0.1, N_f = 1*10^8

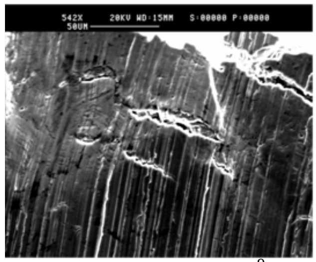
d) R = 0.5, N_f = 8.5*10^9

Fig. 11. Crack path morphology and loading pattern a-b) and crack propagation with crack branching and crack deflection c, d)

Figures 12a to 12f show SEM micrographs of the fracture surfaces of the specimens failed in 3P-bending fatigue tests in gigacycle range at the stress ratio of R= 0.1. In the gigacycle range (>10^8), fracture mode is predominantly cleavage translamellar with very large facet sizes in γ phase. Main cracks with short secondary cracks are also observed in the specimens studied here.

Figure 13a-d illustrate SEM micrographs of the fracture surfaces of the specimens failed in 3P-bending fatigue tests in gigacycle range at the stress ratio of R=0.5. Many small cracks have been observed at the beginning but never propagated due to microstructural barriers such as harder α - Ti_3Al laths and they were always arrested in very narrow lath spacing. In fact, coexistence of the two phases, hard α and soft γ caused this phenomenon.

These observations are agreed with former results [4, 5, 9, 10, 11, 12, 13 and 14] that there is no crack closure in this alloy due to the small size of crack. If the fatigue damage results are compared with the specimens failed at lower stresses in higher fatigue lives ($N_f > 10^8$) give mainly common aspects such as the same crack size and large cleavage facets and only a few internal or subsurface damage initiation are observed. However, these observations can not be detected in the low and medium fatigue ranges.

Shortly, fracture surface is perpendicular and also parallel to the lamellar laths, which introduced very large flat fracture surfaces as displayed in Figures 10, 12 and 13. Moreover, the cleavage patterns on the fracture surfaces are generally observed in γ phase side. Thus, the locations of the crack nucleation should be expected at γ/α interfaces.

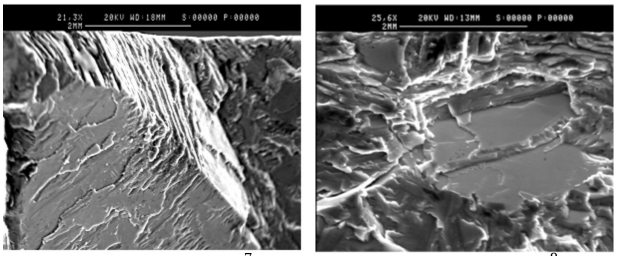

a) R = 0.1, $N_f = 5{*}10^7$ b) R = 0.1, $N_f = 1.5{*}10^8$

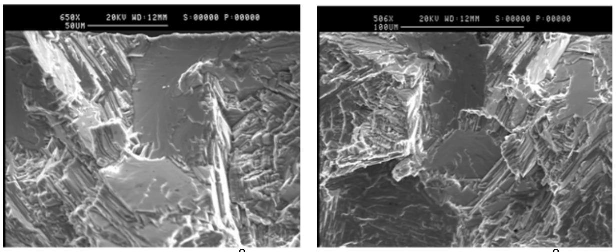

c) R = 0.1, $N_f = 2{*}\ 10^8$ d) R = 0.1, $N_f = 2{*}10^8$

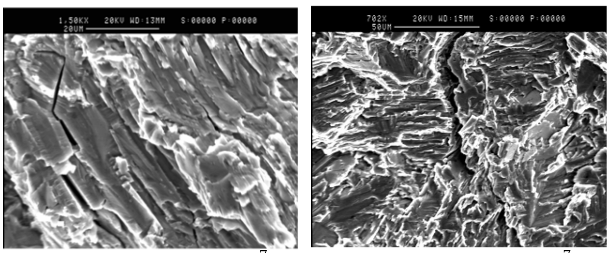

e) R = 0.1, $N_f = 7.9{*}10^7$ f) R = 0.1, $N_f = 8{*}10^7$

Fig. 12. Fracture surfaces of 3P- ultrasonic bending fatigue of the specimens at the stress ratio of R=0.1 with a frequency of 20 kHz

Fatigue fracture surfaces of specimens tested at R= 0.7 have been displayed in Figures 14 and 15. As can be seen clearly from these pictures and figure 7, most of the specimen failures have been obtained in the fatigue range of 10^5-10^7cycles. And majority of the fatigue initiations have been observed from the specimen surface at these conditions.

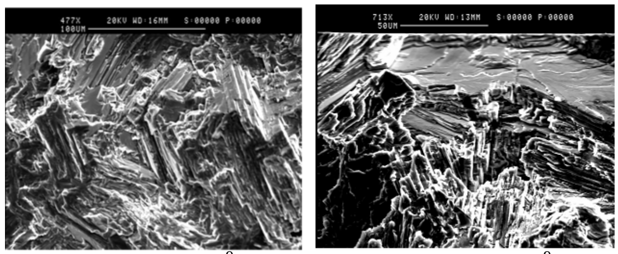

R = 0.5, $N_f = 4{*}10^9$ R = 0.5, $N_f = 1.6{*}10^9$

Fig. 13. SEM micrographs; the fracture surfaces in 3P-bending ultrasonic fatigue range and R=0.5

In fact, it is reasonably, the nominal peak stress is near to the maximum bending stress at the stress ratio R= 0.7. As well discussed in the section of 5.3 and Figure 6, there is no considerable effect of the surface roughness conditions on the fatigue behaviour at the stress ratio of R= 0.7.

In summary, for the specimens failed in the ranges of 10^5-10^7 cycles, fracture initiations have always occurred from the surface of specimen, parallel to the lamellar. For the higher fatigue ranges, the fracture surfaces show large facets (Figure 14.

The fracture surface of the specimen with medium roughness indicates the same fatigue fracture characteristic comparing with the fine roughness surface specimen. Surface fatigue initiation with facet and crack growth in the translamellar pattern is observed in Figure 14.

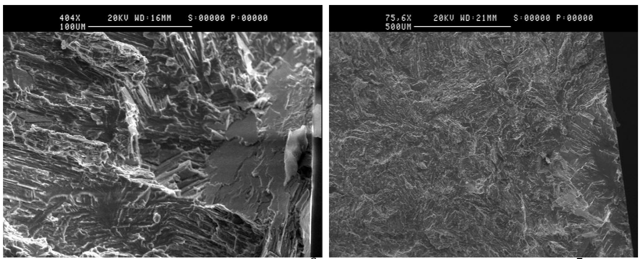

a) fine surface N_f=1.45x10^6 b) fine surface N_f=3.4x10^5

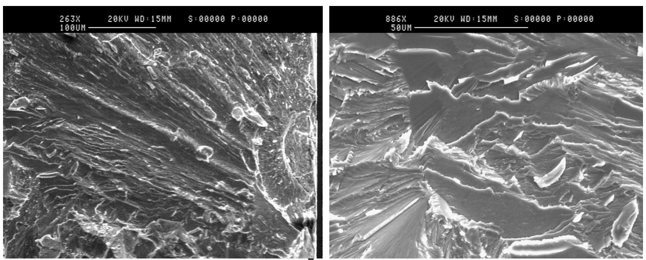

c) medium surface; N_f=7.95x10^5 d) idem c

Fig. 14. a, b and c Fatigue initiation and short propagation zones at the stress ratio of R=0.7 in different surface roughness conditions

For the specimens failed in the higher cycle fatigue ranges, damage initiation was observed from the subsurface (Figure 15).

Additionally, the fatigue fracture surface with coarse roughness surface showed the same damage behaviour as fine surface specimen. However, multiple fatigue initiation sites on the surface can be often observed at the low cycle fatigue ranges. Furthermore, many secondary cracks were regularly detected on the specimen surfaces in the low cycle ranges.

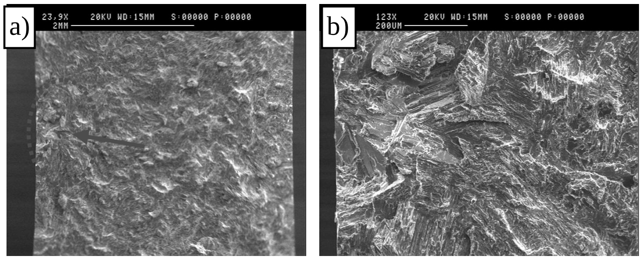

Fig. 15. Fatigue initiation and propagation at subsurface a) with cleavage surface b), (medium surface R=0.7, $N_f = 6.27x10^7$)

6. Conclusions

Two-phase (α_2+γ) Ti-Al based intermetallics alloy has been manufactured and damage mechanisms were investigated under different test conditions; static tensile, 3P bending and also 3P ultrasonic fatigue bending.

Fatigue damage occurs with the formation of the mechanical twin formation in the microstructure (mainly in γ grains and also in lamellar grains) of the specimens tested under high static stress levels and low dynamic cyclic stress conditions. However, more detail TEM investigations should be carried out to well understand the role of the twin and slip band formation on the damage mechanisms. Stress ratio is an important parameter on the fatigue life and fracture mode of this alloy. Dominant fatigue failure mode obtained at room temperature is cleavage translamellar with very large facet sizes in γ phase. The specimens failed at two different stress ratios of R= 0.1 and 0.5 beyond 10^8 give many common results such as the same crack size, very large cleavage facets, etc.. Fracture surface is perpendicular and also parallel to the lamellar laths, which introduce very large fracture surfaces generally observed in γ side. So, the locations of the crack nucleation should be expected mainly at γ/α interfaces. A limited fatigue life is obtained with the stress ratio of R= 0.7. Because the fatigue strength is close to the bending strength in this ratio and naturally the most of the fatigue damage occurred in low cycles fatigue ranges (10^5-10^6 cycles).

References

[1] J.J. Kruzic, J.P. Campbell, O. Ritchie, On the fatigue behaviour of g-based titanium aluminides: Role of small cracks, Acta materialia 47/3 (1999) 801-816.

[2] Y.S. Park, S.W. Nam, S.K. Hwang, N.J. Kim, The effect of the applied strain range on fatigue cracking in lamellar Ti-Al alloy, Journal of Alloys Compounds 335 (2002) 216-223.

[3] J.P. Campbell, R.K.T. Venkateswara, R.O. Ritchie, The effect of microstructure on fracture toughness and fatigue crack growth behaviour in γ-titanium aluminides based intermetallics, Metallurgica Materials Transanction A 30/3 (1999) 565.

[4] J.P. Campbell, J.J. Kruzic, S. Lillibridge, K.T.V. Rao, R.O. Ritchie, On the growth of small fatigue cracks in γ-based titanium aluminides, Scripta Materialia 37/5 (1997) 707-712.

[5] S.J. Zhu, L.M. Peng, T. Moriya, Y. Mutoh, Effect of stress ratio on fatigue crack growth in Ti-Al intermetallics at room and elevated temperatures, Materials Science Engineering A. 290 (2000) 198-206.

[6] J.P. Campbell, R.O. Ritchie, Mixed-mode, high cycle fatigue-crack growth thresholds in Ti-6Al-4V. I. A comparison of large and short-crack behaviour, Engineering of Fracture Mechanics 67 (2000) 209-227.

[7] R. Gnanamoorthy, Y. Mutoh, Y. Mizuhara, Fatigue crack growth behaviour of equiaxed, duplex and lamellar microstructure γ base titanium aluminides, Intermetallics 4 (1996) 525-532.

[8] C. Bathias, C.P. Paris, Gigacycle Fatigue in Mechanical Practice, Marcel Dekker Inc. 2004; ISBN:0-8247-2313-9; DK3165.

[9] E. Bayraktar, C. Bathias, H. Xue, H. Tao, On the Giga Cycle Fatigue Behaviour of two-phase (α_2 + γ) Ti-Al Alloy, Internationa Journal of Fatigue 26/2 (2004) 1263-1275.

[10] H. Xue, E. Bayraktar, C. Bathias, Effect of ultrasonic fatigue specimen geometry on its strain field and heat response, Proceedings of the 11th International Scientific Conference on the "Contemporary Achievements in Mechanics, Manufacturing and Materials Science" CAM3S'2005, Gliwice-Zakopane, 2005, 1049-1055.

[11] B. Skrotzki, M. Ünal, G. Eggeler, On the role of mechanical twinning in creep of a near-γ Ti-Al-alloy with duplex microstructure, Scripta Materialia 39/8 (1998) 1023-1029.

[12] W. Schillinger, B. Lorenzen, A. Bartels, Anisotropic mechanical behaviour of textured γ-Ti-Al caused by the directionality of twinning, Materials Science Engineering A 329-331 (2002) 644-648.

[13] W.Z. Chen, X.P.K. Song, W. Qian, H.C. Gu, The lamellar microstructure and fracture behaviour of γ–based Ti-Al alloy produced by centrifugal spray deposition, Materials Science Engineering A 247/1-2 (1998) 126-134.

[14] M.A. Morris, Deformation mechanism in fine-grained Ti-Al alloys, Materials Science Engineering A224 (1997) 12-20.

[15] S.A. Satyam, K. Singh, R.K. Ray, S. Bhargava, Textural changes during thermomechanical processing of Ti-24Al-11Nb alloy, Scripta Materialia 35/7-1 (1996) 897-902.

[16] G. Jago, Relations entre paramètres microstructuraux et mécanismes d'endommagement des alliages de titane α+β forge. Application à l'alliage de titane Ti6246 en fatigue vibratoire à 20kHz. PhD Thesis, ITMA/CNAM, 1996.

[17] Z.D. Sun, Q.Y. Wang, C. Bathias, Experimental investigation on freeting fatigue of high strength steel at ultrasonic frequency. FATIGUE'99 Proceeding of the 7th International Fatigue Congress. Beijing, China, 1999, 1365-1370.

[18] C. Kanchanomai, Y. Miyashita, Y. Mutoh, S.L. Mannan, Influence of frequency on low cycle fatigue behavior of Pb-free solder 96.5Sn–3.5Ag, Materials Science and Engineering A345 (2003) 90-98.

[19] X.Q. Shi, H.L.J. Pang, W. Zhou, Z.P. Wang, Low cycle fatigue analysis of temperature and frequency effects in eutectic solder alloy, International Journal of Fatigue 22 (2000) 217-228.

[20] H. Xue, Explanation of Gigacycle Fatigue of Materials in Tension, Bending and Torsion Loading, PhD Thesis, ITMA/CNAM, 2005.

[21] X. Kong, K. Saanouni, C. Bathias, On the fatigue at very high frequency, part 1: Theoretical and variation formulation, Journal of Engineering Materials and Technology 113 (1991) 205-209.

[22] X. Kong, Theoretical and numerical study of ultrasonic fatigue, PhD Thesis, UTC (1988).

[23] S. Purushothaman, High power ultrasonic fatigue. Proc.UI-1973, 244.

[24] H.R. Mayer, D.M. Tan, S.E. Stanzl-Tschegg, FEM modelling of stress intensity factors during fatigue crack growth at ultrasonic frequencies Engineering of Fracture Mechics 45 (1993) 487-495.